ARTICLES

Bio-friendly Synthesis of ZnO Nanoparticles in Aqueous Solution at Near-Neutral pH and Low Temperature

Luciana Pitta Bauermann,* Joachim Bill, and Fritz Aldinger

Max-Planck-Institut für Metallforschung and Institut für Nichtmetallische Anorganische Materialien, Universität Stuttgart, Pulvermetallurgisches Laboratorium, Heisenbergstr. 3, D-70569 Stuttgart, Germany

Received: November 24, 2005; In Final Form: January 24, 2006

ZnO nanoparticles are synthesized using a new bio-friendly method. The experimental conditions are very mild: aqueous solution at near-neutral pH and 37 °C. The as-obtained nanoparticles show the stable wurtzite structure without the need of annealing. The two reagents used are aqueous solutions of zinc nitrate and buffer tris(hydroxymethyl)aminomethane. This is a standard nontoxic buffer and inert to a wide variety of chemicals and biomolecules, therefore extremely satisfactory for biochemical reactions. Furthermore, this is a polydentade ligand which adsorbs strongly on one or more surfaces of ZnO inhibiting its crystal growth and yielding nearly spherical ZnO nanoparticles. Our objective is to use the crystallization method described here for further incorporation of biomolecules as additives in the reaction solution, aiming at the formation of ZnO with new physical properties.

Introduction

The perspective of developing new materials by combining biological and inorganic components has caused rising interest in many scientific groups.[1−3] There are different biomolecules which can be incorporated into inorganic substances yielding materials with new properties not yet synthesized. A requirement for this successful association is the use of bio-friendly, mild experimental conditions, because biomolecules are very sensitive to changes in temperature and pH. We describe a new, simple, fast, and cheap procedure for the synthesis of high-quality ZnO nanoparticles in aqueous solution at pH close to neutral and physiological temperature. A few methods for obtaining ZnO nanocrystals or nanorods in aqueous solution at low temperature have been reported, but they all involve strong alkaline media[4−7] or annealing.[8] In our new process, only two reagents are necessary for the ZnO crystallization: zinc nitrate and the buffer tris(hydroxymethyl)aminomethane. This buffer has an elevated buffering capacity, is promptly soluble in water, and is inert in a variety of enzymatic reactions therefore particularly suitable for biological purposes.[9] Additionally, this is a tridentate ligand, providing specific metal binding sites.[10,12] This poly(alcohol)-amine adsorbs on one or more surfaces of the ZnO inhibiting crystal growth and generating slightly anisotropic nanocrystallites. Tris(hydroxymethyl)aminomethane has been previously used on the synthesis of TiO_2 nanocrystals. But in this case, this buffer was dispersed in benzyl alcohol and heated at 80 °C,[11] a process not compatible with our bio-friendly purposes. Tris(hydroxymethyl)alkanes have already been combined with group IV metal alkoxides, yielding complex ceramic precursors.[12]

* To whom correspondence should be addressed. Tel: +49(0)711 689 3231. Fax: +49(0)711 689 3131. E-mail: pitta@mf.mpg.de.

Experimental Section

ZnO nanoparticles were prepared by adding a specific volume of 500 mM $Zn(NO_3)_2(H_2O)_6$ to a final concentration of 20 mM, into 30 mM buffer tris(hydroxymethyl)aminomethane at pH 8 (1.842 g/L Trizma HCl and 2.22 g/L Trizma base). The reaction took place in an incubator maintained at 37 °C for 4 h. The obtained precipitate was then washed with deionized water, centrifuged, and dried at 37 °C in air. The chemicals used are reagent grade from Sigma Aldrich. The ZnO as-obtained was divided in four parts. One part was kept at 37 °C, and the other three were heated for 2 h at 80, 600, and 1000 °C. The heat treatment was performed in air using a heating rate of 10 °C/min. The samples were then characterized using scanning electron microscopy (SEM) (Zeiss DSM 982), transmission electron microscopy (TEM) (JEM 2000 FX), and Fourier transform infrared spectroscopy (FTIR) (Nicolet, Avatar 360 FTIR spectrometer). For the FTIR experiments, the ZnO samples were ground with KBr (spectroscopic grade powder, Graseby Specac Ltd.) and pressed to pellets.

The release of the oxidized gas species H_2O, CO_2, and NO from the as-obtained ZnO was monitored by a thermogravimetry/mass spectrometer, TG/MS (Netzch 449C and InProcess Instruments GAM 200). The sample was heated in a Pt crucible to 1000 °C in air using a heating rate of 10 °C/min.

X-ray powder diffraction (XRD) patterns were recorded using a Philips X'Pert MPD diffractometer applying Bragg−Brentano geometry and a primary beam monochromator to select the $K\alpha_1$ component of the employed copper radiation (wavelength of 1.54056 Å). The samples consisted of thin layers of the ZnO powders deposited onto single crystalline silicon wafers with a (510) plane parallel to the surface. To determine the instrumental resolution of the diffractometer, measurements on a LaB_6 powder specimen (NIST standard 660a) were made. Parameters

10.1021/jp056830m CCC: $33.50
Published on Web 02/18/2006

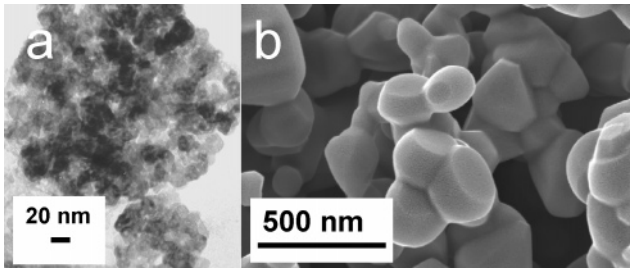

Figure 1. (a) Bright-field transmission electron micrograph of as-obtained ZnO nanoparticles precipitated in aqueous solution at pH 8 and 37 °C and (b) scanning electron micrograph of ZnO particles after heat treatment in air at 1000 °C for 2 h.

describing the instrumental profile were fitted to the LaB_6 data by employing the fundamental parameters approach using the TOPAS package.[13] The physical diffraction-line broadening of each ZnO reflection of each sample was determined by convoluting the instrumental resolution at the reflection position $2\theta_{hkl}$ with a pseudo-Voigt function with a fitted full width at half maximum and peak-shape factor, from which the integral breadth, β_{hkl}, can be calculated. These integral breadth values with hkl = 100, 002, 101, 102, 110, 103, 200, 112, and 201 were incorporated into Williamson Plots[14] $\beta_{hkl} \cos \theta_{hkl}/\lambda$ vs $2 \sin \theta_{hkl}/\lambda$ for each sample, yielding measurements for crystallite size D and microstrain, e

$$\frac{\beta_{hkl} \cos \theta_{hkl}}{\lambda} = \frac{4e \sin \theta_{hkl}}{\lambda} + \frac{1}{D}$$

For the determination of the lattice parameters, mixtures of the ZnO samples and silicon powder (with lattice parameter a = 5.43102 Å) were placed together onto adhesive tape and investigated on a FR552 Guinier camera (Enraf Nonius, Delft (NL), transmission geometry, working with Cu $K\alpha_1$ radiation, λ = 1.54056 Å). Reflection positions were extracted using the TOPAS package.[13] The positions of the ZnO reflections were corrected on the basis of those of the Si reflections and used as input for fitting the hexagonal lattice parameters a and c of ZnO applying the program U-Fit.[15]

Results and Discussion

Figure 1 shows the transmission electron micrograph of the ZnO nanoparticles as-obtained and the scanning electron micrograph of the ZnO sintered in air at 1000 °C. According to the micrographs, the as-obtained nanoparticles and the sintered ones have mean diameters of approximately 20 and 300 nm, respectively. The increase in particle size is a known phenomenon for ceramics upon heating.[16] The ZnO nanoparticles achieved here are nearly spherical with some faceting. This morphology is unusual for ZnO and is obtained most probably because the poly(alcohol)amine buffer is a polydentade ligand and adsorbs strongly on the crystalline surfaces inhibiting its crystal growth.[11]

Figure 2 shows X-ray diffraction patterns of the ZnO samples treated at different temperatures. ZnO as-obtained maintained at 37 °C is crystalline and shows a stable wurtzite structure. It is important to mention that even performing the synthesis at 4 °C, wurtzite ZnO is obtained as the only crystalline product. The reflections of ZnO turn sharper by heating the sample in air at temperatures higher than 37 °C. This result could be caused by the increase in crystalline size seen in Figure 1 but could also be a consequence of a reduction of microstrain broadening. Williamson−Hall plots shown in Figure 3 suggest that size broadening is the main parameter, however the microstrain

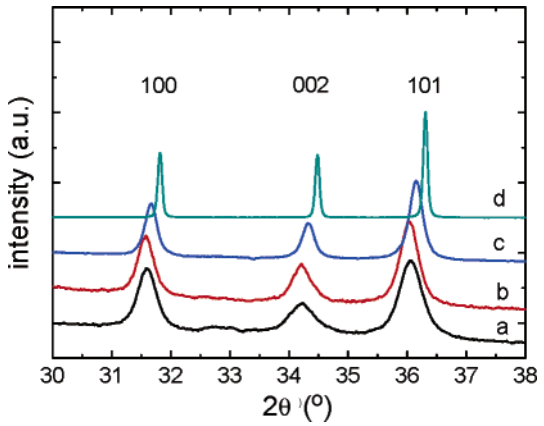

Figure 2. X-ray powder diffraction patterns of ZnO nanoparticles precipitated in aqueous solution at pH 8 and 37 °C thermally treated in air at (a) 37 °C, (b) 80 °C, (c) 600 °C, and (d) 1000 °C.

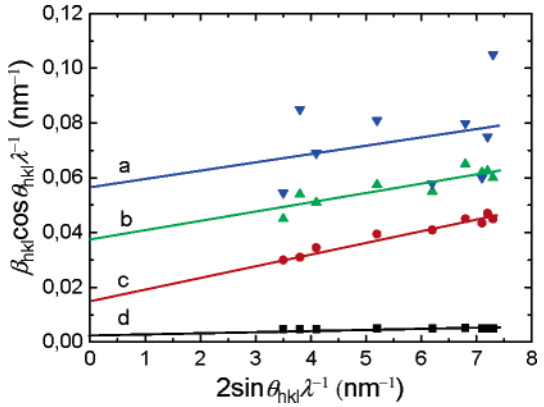

Figure 3. Williamson−Hall plots for analysis of the diffraction-line broadening of ZnO nanoparticles precipitated in aqueous solution at pH 8 and 37 °C thermally treated in air at (a) 37 °C, (b) 80 °C, (c) 600 °C, and (d) 1000 °C. The straight lines give linear fits considering all reflections, whereas the dashed line represents a fit exclusively based on the (hk0) reflections of the 37 °C, which show pronounced anisotropy.

TABLE 1: Data Resulting from X-ray Diffraction Analysis of ZnO Synthesized at 37 °C, Divided into Four Parts, and Subsequently Thermally Treated in Air at 37, 80 , 600, and 1000 °C[a]

T (°C)	a (Å)	c (Å)	V (Å^3)	D (nm)	10^3e
37	3.2556(3)	5.2169(10)	47.890(2)	18(6)[b]	3.0(3)[b]
80	3.2525(3)	5.2098(10)	47.730(2)	27(3)	3.4(7)
600	3.2500(4)	5.2059(10)	47.620(8)	63(9)	4.1(4)
1000	3.2490(1)	5.2038(3)	47.572(6)	290(50)	0.32(10)

[a] Lattice parameters, a and c, volume of unit cell, V, axial ratio, c/a, average crystallite size, D, and microstrain, e, from Williamson−Hall Plots. [b] High standard deviations are due to the strong scatter of data points caused by anisotropy of the line broadening. A separate evaluation of the line broadening of the (hk0) reflections yields D = 21.0(4) nm and e = 0.0017(2).

broadening cannot be neglected. The calculated crystalline sizes, displayed in Table 1, agree well with the ones observed in Figure 1. The strong scatter of the data from the ZnO maintained at 37 °C indicates that the line broadening is caused by size anisotropy or microstrain anisotropy (see, e.g., difference of the extent of line broadening for the reflections with hkl = 100 and 002, having similar diffraction angles). A closer analysis hints at size anisotropy, where the crystals' average extension along the [uv0] direction is larger by a factor of about 1.5 than along the [00w] direction. This anisotropy can be caused by the adsorption or desorption of the buffer assembler on specific

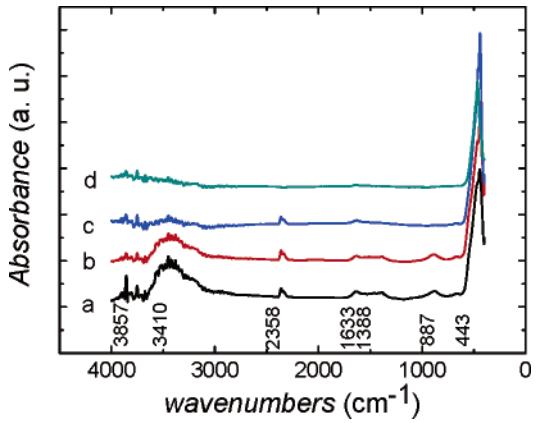

Figure 4. Room-temperature FTIR absorption spectra of ZnO nanoparticles precipitated in aqueous solution at pH 8 and 37 °C thermally treated in air at (a) 37 °C, (b) 80 °C, (c) 600 °C, and (d) 1000 °C.

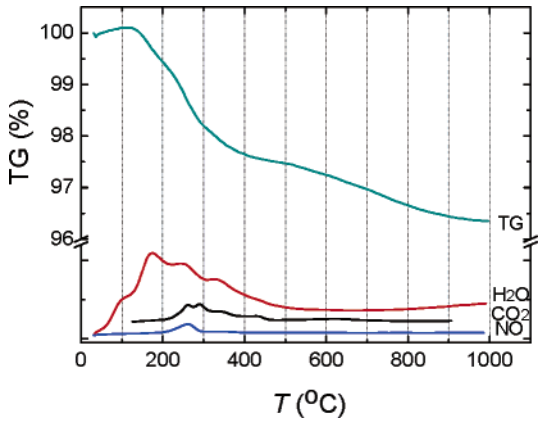

Figure 5. Thermogravimetric measurements by heating in air the as-synthesized ZnO nanoparticles up to 1000 °C using a heating rate of 10 °C/min, coupled to a mass spectrometer for the detection of the oxidized gas species: H_2O, CO_2, and NO.

surfaces of the ZnO. This ratio is larger than the values found for nanocrystalline ZnO obtained from different solid-state precursors showing, if any size anisotropy was found at all, that the size along the [00*w*] direction is usually larger than that along the [*uv*0] direction.[17,18] The presently observed results on the anisotropy of the line broadening are also in agreement with the literature[18] concerning the fact that the degree of anisotropy is significantly leveled upon the grain growth that occurs upon annealing. The anisotropy is present to a much less extent, if at all, for the samples annealed at temperatures equal to or higher than 80 °C.

The lattice parameters of the wurtzite phase, *a* and *c*, and the volume of the unit cell, *V*, are calculated from Si-calibrated Guinier data for the ZnO nanoparticles subjected to different temperatures, and the results are shown also in Table 1. By exposing the ZnO crystals to high temperatures, the volume of the unit cells, *V*, decreases. This shrinkage of the unit cell volume is very considerable when the ZnO is heated from 37 to 600 °C (contraction from $V = 47.90$ Å^3 to $V = 47.62$ Å^3). These values do not decrease much with further increase in temperature ($V = 47.60$ Å^3 for 1000 °C). At this point, we propose that this reduction in volume is caused by a loss of ions, which were eventually trapped in the ZnO crystalline structure, for example, hydrogen or oxygen. To check this hypothesis, we analyzed the ZnO samples treated at different temperatures using FTIR and TG/MS.

FTIR spectra of the ZnO samples are shown in Figure 4. The typical IR absorption peak of ZnO is found at about 443 cm^{-1} in all four curves and also the CO_2 atmospheric peak at 2358 cm^{-1}. For the samples kept at low temperature (parts a and b of Figure 4 maintained respectively at 37 and 80 °C), there are extra peaks indicating the bonds of N−H at 1633 cm^{-1}, C−H at 1388 cm^{-1}, and O−H at 3410 cm^{-1}, originating from the organic buffer and, perhaps, water adsorbed on the surface of the nanocrystallites. Because the buffer is decomposed at 219 °C, those peaks disappeared when the ZnO samples were annealed in air at 600 and 1000 °C (parts c and d of Figure 4).

Thermogravimetry/mass spectrometry (TG/MS) measurements were performed to investigate the thermal stability of the assembler-buffer adsorption on the ZnO nanoparticles and to investigate the reason for the ZnO unit cell shrinkage upon heating. The experiments were realized in air with the temperature increasing from room temperature to 1000 °C at a rate of 10 °C/min with a simultaneous detection of the oxidized evaporated species by a coupled mass spectrometer. Figure 5 shows a continuous mass loss of the ZnO by increase in temperature, with a higher slope between 150 and 350 °C. The observed weight loss at temperatures higher than 400 °C corresponds to the baseline of the equipment. Four peaks of H_2O, two of CO_2, and one of NO are detected by the mass spectrometer. H_2O vapor registered at 246 and 333 °C, CO_2 at 260 and 288 °C, and NO at 272 °C come from the degradation of the assembler-buffer tris(hydroxymethyl)aminomethane, $C(CH_3OH)_3NH_2$, which boils at 219 °C at 10 mmHg.[19] The H_2O peak recorded at 100 °C originated from the adsorbed water on the ZnO particles. The second H_2O peak, detected by the mass spectrometer at 173 °C, is correlated with the decomposition of $Zn(OH)_2$, which theoretically occurs at 130 °C.[20] From the XRD measurements (Figure 2), no presence of crystalline $Zn(OH)_2$ is observed. Thus, the $Zn(OH)_2$ present is amorphous or these are hydrogen-doped ZnO formed due to the large amount of hydrogen found in the crystal growth environment.

ZnO is known to be doped with hydrogen positively charged placed as interstitials.[21] These protons can be situated either between the O and Zn atoms or antibonding to oxygen in the wurtzite-type lattice. The latter is analogous to the hydroxyl site, which is common in oxides.[16,22] This proton implantation in the ZnO wurtzite structure is accompanied by remarkably large relaxations of the surrounding atoms[21] increasing the length of the bond between zinc and oxygen.[23] The interstitial hydrogen in the ZnO is not thermally stable and leaves the crystalline structure when heated.[24] The water peak detected at 173 °C by the TG/MS experiment shown in Figure 5 is an indication of the presence of the interstitial hydrogen which is oxidized in air to water. This loss of protons is in accordance with the calculated shrinkage of the volume of the ZnO unit cell, which occurred upon heating (Table 1). Hydrogen-doped ZnO have interesting technological applications, and they were already synthesized artificially and analyzed by photoluminescence and IR spectroscopy,[25,26] Raman backscattering spectroscopy,[27] and conductivity measurements.[23]

At this point, we propose the following mechanism of nucleation and growth of the ZnO nanoparticles. The dissolved zinc nitrate hexahydrate forms an aquo complex with Zn^{2+} cations as the center particle and "coordinating" water "ligands". The electron density is attracted to the direction of the zinc cation and moves further away from the O−H bond, making the ionization of water easier.[28] The assembler buffer consumes the protons released, increasing the rate of the hydrolysis of the zinc complex at low temperature and allowing only a small decrease in the pH solution. The deprotonated zinc complex acts as a nucleophile and binds to zinc cations from other

molecules of the zinc−water complex forming ZnO with an excess of protons (eq 1). This olation-type reaction has already been proposed for the formation of metal oxides in water,[28] where there is the formation of an "ol" bridge between the metal ions.

$$M-OH + M-H_2O \rightarrow M-OH-M + H_2O \qquad (1)$$

Some of the protons are further consumed by the buffer, yielding the ZnO wurtzite type with some interstitial protons (eq 2). These interstitial protons leave the crystalline structure by heating at 173 °C (showed in the lattice parameters calculation and thermogravimetric experiments).

$$M-O(H)_1-M \rightarrow M-O(H)_{1-y}-M + (y)H^+ \quad 0 < y < 1 \qquad (2)$$

Conclusion

In summary, we reported a new method to synthesize ZnO nanoparticles in aqueous solution at near-neutral pH and body temperature. The nanosized crystals obtained by this simple technique are crystalline without the need of annealing and nearly spherical in shape. The tris(alcohol)amine used as a buffer also acts as poly(dentate) binding to the zinc oxide limiting its crystal growth. The buffer increases the rate of hydrolysis of the zinc−water complex by consuming protons yielding a ZnO wurtzite type with some protons trapped in the interstitial sites. These protons leave the crystalline structure by heating at about 180 °C, causing a decrease in the unit cell volume of ZnO. Our aim is to use this method of bio-friendly synthesis to create new hybrids of ZnO by introducing biomolecules during the crystallization.

Acknowledgment. The authors gratefully acknowledge Andreas Leineweber (ZWE) for the X-ray diffractometry and Guinier method analyses, Gerhard Kaiser for performing thermogravimetric experiments, Hartmut Labitze for the SEM images, Peter Kopold for the TEM investigation, and Peter Gerstel for laboratory assistance.

References and Notes

(1) Aizenberg, J. *Adv. Mater.* **2004**, *16* (15), 1295−1302.
(2) Coradin, T.; Livage, J. *Mater. Sci. Eng., C* **2005**, *25*, 201−205.
(3) Cölfen, H.; Mann, S. *Angew. Chem., Int. Ed.* **2003**, *42*, 2350−2365.
(4) Jin, C. F.; Yuan, X.; Ge, W. W.; Hong, J. M.; Xin, X. Q. *Nanotechnology* **2003**, *14*, 667−669.
(5) Tian, Z. R.; Voigt, J. A.; Liu, J.; McKenzie, B.; McDermott, M. J.; Rodriguez, M. A.; Konishi, H.; Xu, H. *Nat. Mater.* **2003**, *2*, 821−826.
(6) Wang, Z.; Qian, X.-F.; Yin, J.; Zhu, Z.-K. *Langmuir* **2004**, *20*, 3441−3448.
(7) Ristić, M.; Musiæ, S.; Ivanda, M.; Popoviæ, S. *J. Alloys Compd.* **2005**, *397*, L1−L4.
(8) Hoffmann, R.; Fuchs, T.; Niesen, T. P.; Bill, J.; Aldinger, F. *Surf. Interface Anal.* **2002**, *34*, 708−711.
(9) Good, N. E.; Winget, G. D.; Winter, W.; Connolly, T. N.; Izawa, S.; Singh, R. M. M. *Biochemistry* **1966**, *5* (2), 467−477.
(10) Cornia, A.; Gatteschi, D.; Hegetschweiler, K.; Hausherr-Primo, L.; Gramlich, V. *Inorg. Chem.* **1996**, *35*, 4414−4419.
(11) Polleux, J.; Pinna, N.; Antonietti, M.; Hess, C.; Wild, U.; Schlögl, R.; Niederberger, M. *Chem.−Eur. J.* **2005**, *11*, 3541−3551.
(12) Boyle, T. J.; Schwartz, R. W.; Doedens, R. J.; Ziller, J. W. *Inorg. Chem.* **1995**, *34*, 1110−1120.
(13) *TOPAS, General Profile and Structure Analysis Software for Powder Diffraction Data*, version 2.0.
(14) Williamson, G. K.; Hall, W. H. *Acta Metall.* **1953**, *1*, 22−31.
(15) Evain, M. *U-fit program*; Institute des Materiáux de Nantes: Nantes, France, 1992.
(16) Kingery, W. D. *Introduction to Ceramics*; Wiley & Sons: New York, 1976.
(17) Louër, D.; Auffrédic, J. P.; Ciosmak, D.; Niepce, J. C. *J. Appl. Crystallogr.* **1983**, *16*, 183−191.
(18) Audebrand, N.; Auffrédic, J. P.; Louër, D. *Chem. Mater.* **1998**, *10*, 2450−2461.
(19) Safety data sheet of tris(hydroxymethyl)aminomethane, Aldrich.
(20) *Handbook of Chemistry and Physics*, 85th ed.; Lide, D. R., Ed.; CRC Press: Boca Raton, FL, 2004−2005.
(21) Walle, C. G. V. d. *Phys. Rev. Lett.* **2000**, *85* (5), 1012−1015.
(22) Cox, S. F. J.; Davis, E. A.; Cottrell, S. P.; King, P. J. C.; Lord, J. S.; Gil, J. M.; Alberto, H. V.; Vilão, R. C.; Duarte, J. P.; Campos, N. A. d.; Weidinger, A.; Lichti, R. L.; Irvine, S. J. C. *Phys. Rev. Lett.* **2001**, *86* (12), 2601−2604.
(23) Seager, C. H.; Myers, S. M. *J. Appl. Phys.* **2003**, *94* (5), 2888−2894.
(24) Ip, K.; Overberg, M. E.; Heo, Y. W.; Norton, D. P.; Pearton, S. J.; Kucheyev, S. O.; Jagadishi, C.; Williams, J. S.; Wilson, R. G.; Zavada, J. M. *Appl. Phys. Lett.* **2002**, *81* (21), 3996−3998.
(25) Lee, J.-K.; Nastasi, M.; Hamby, D. W.; Lucca, D. A. *Appl. Phys. Lett.* **2005**, *86*, 171102.
(26) McCluskey, M. D.; Jokela, S. J.; Zhuravlev, K. K.; Simpson, P. J.; Lynn, K. G. *Appl. Phys. Lett.* **2002**, *81* (20), 3807−3809.
(27) Nickel, N. H.; Fleischer, K. *Phys. Rev. Lett.* **2003**, *20* (19), 197402.
(28) Govender, K.; Boyle, D. S.; Kenway, P. B.; O'Brien, P. *J. Mater. Chem.* **2004**, *14*, 2575−2591.